ACS OMEGA

Article

Cite This: ACS Omega 2019, 4, 3169−3177

http://pubs.acs.org/journal/acsodf

Methylene Blue-Loaded Upconverting Hydrogel Nanocomposite: Potential Material for Near-Infrared Light-Triggered Photodynamic Therapy Application

Brahmaiah Meesaragandla,[†,‡] Debashrita Sarkar,[†,‡] and Venkataramanan Mahalingam*[,†,‡]

[†]Department of Chemical Sciences and [‡]Center for Advanced Functional Materials (CAFM), Indian Institute of Science Education and Research (IISER) Kolkata, Mohanpur, West Bengal 741252, India

Supporting Information

ABSTRACT: The property of upconverting nanoparticles to convert the low-energy near-infrared (NIR) light into high-energy visible light has made them a potential candidate for various biomedical applications including photodynamic therapy (PDT). In this work, we show how a surface functionalization approach on the nanoparticle can be used to develop a nanocomposite hydrogel which can be of potential use for the PDT application. The upconverting hydrogel nanocomposite was synthesized by reacting 10-undecenoic acid-capped Yb^{3+}/Er^{3+}-doped $NaYF_4$ nanoparticles with the thermosensitive *N*-isopropylacrylamide monomer. The formation of hydrogel was completed within 15 min and hydrogel nanocomposites showed strong enhancement in the visible light emission compared to the emission obtained from 10-undecenoic acid-capped Yb^{3+}/Er^{3+}-doped $NaYF_4$ nanoparticles via the upconversion process (under 980 nm laser excitation). The upconverting hydrogel nanocomposites displayed high swelling behavior in water because of their porous nature. The porous structure ensured a higher loading of methylene blue dye (∼78% in 1 h) into the upconverting hydrogel, which was achieved via the swelling diffusion phenomenon. Upon excitation with the NIR light, the visible light emitted from the hydrogel activated the photosensitizer methylene blue which generated reactive oxygen species. Our results were able to show that the methylene blue-loaded composite hydrogel can be a potential platform for the future of NIR-triggered PDT in skin cancer treatment.

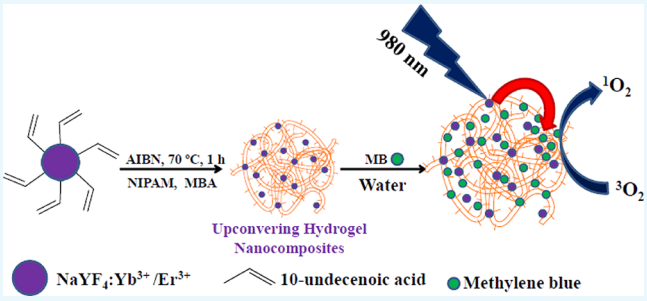

INTRODUCTION

Photodynamic therapy (PDT) is the technique which is well known in the diagnosis of dermatosis and even malignant cancer.[1−4] This technique uses a suitable source of light and a photosensitizer (PS) molecule for the formation of reactive oxygen species (ROS) which are responsible for the cell death.[5−8] The basic principle of PDT is the activation of the PS molecule via the light of suitable wavelength. The PS molecule, in turn, generates the ROS which causes oxidative cell damage to the particular tissue.[9,10] To explain the phenomenon briefly, first, the PS molecule is administered to the particularly affected tissue in the absence of light, after which the PS molecule distributes itself in the particular area. When light is irradiated on the affected tissue, the PS generates ROS facilitating cell death. In conventional PDT, the PSs used are predominantly activated by visible light. Visible light has its own limitation of passing through the thick tissue membrane, and therefore it is a challenge to minimize the loss of light. The higher penetration behavior of near-infrared (NIR) light over visible light into the skin tissue is an advantage for NIR-responsive material to be applied for PDT as the NIR light-triggered material would give a higher signal to noise ratio with low autofluorescence.[11] To facilitate this technique, a suitable transducer can be utilized to convert NIR light to visible light. The generated visible light will effectively activate the PSs which are usually visible light-responsive materials. For an effective PDT, the PSs must satisfy two conditions. First, they should be target-specific to the tissue of interest. Second, they should be able to efficiently generate the ROS when irradiated with a suitable light source.

The process of conversion of NIR to visible light can be easily achieved using lanthanide-doped upconverting nanomaterials.[12−23] Lanthanide ions (Ln^{3+}) are known to possess the ability to convert lower energy light into higher energy light via a nonlinear multiphoton process called anti-Stokes process. In addition, these nanoparticles (NPs) are an interesting luminescent probe because of their properties such as nonblinking emission, excellent photostability, low autofluorescence background, and deep tissue penetration of light into biological systems with comparatively lower toxicity and higher luminescence lifetime enabling longer particle tracking.[24−31] Thus, upconverting NPs are an interesting choice for applications in biomedical areas, especially as a nanotransducer. It helps to overcome the problems that traditional

Received: September 18, 2018
Accepted: December 25, 2018
Published: February 13, 2019

DOI: 10.1021/acsomega.8b02416
ACS Omega 2019, 4, 3169−3177

photodyanamic therapy has been facing so far.[32,33] The visible light emitted by the excitation of NIR light is able to trigger the PS dye molecule via resonance energy transfer to generate singlet oxygen species if the absorption window of PS matches with the emission window of upconverting NPs. Thus, NIR light-stimulated upconverting NPs potentially open new doors to PDT. In principle, the PSs should be in the vicinity of the upconverting NPs for efficient energy transfer. Ideally, higher the overlap between the absorption of the PS and the emission from the upconverting NP, the higher will be the efficiency of singlet ($^1O_2$) generation.

There are quite a few reports where various PS molecules are loaded into silica, polymer-coated and core/shell upconverting NPs.[34−44] However, the number of PS molecules attached to these coated NPs is quite low because of less porosity. For example, Xu et al. have shown that 29% of PS loading is achieved for the core/shell dumbbell-like $NaYF_4:Yb^{3+}/Er^{3+}$@$NaNdF_4:Yb^{3+}$ NPs.[45] In the case of polymer-coated NPs, 22.5% of PS loading is observed.[46] In another study, the loading capacity of PS for silica-coated $NaYF_4$:Er/Yb/Gd NPs was experimentally calculated to be 0.05 mmol methylene blue (MB)/UCNP.[47] Recently Huang et al. have shown the combined photothermal and photodynamic effect by integrating silica NPs with upconverting NPs and gold nanorods.[48] They have used zinc phthalocyanine as sensitizers. Although, the PS loading was very high. Moreover, PS may not be stable on the NP surface because of weak interactions and can be isolated from the NPs quickly, thus reducing the PDT efficiency. One way to circumvent this issue is to use hydrogels as a platform to study the PDT. Hydrogel-based materials have been shown as a potential drug-delivery candidate because of their stimuli-responsive nature and porous structure. The shape and behavior of the porous patterns can be tuned in such a way that it can store multiple numbers of drugs selectively. The ROS generated by the PS molecule can be easily released out of the porous hydrogel system as opposed to dense silica and polymer coating.[49−51] Keeping these in mind, attaching an upconverting nanomaterial with a suitable hydrogel can be really advantageous to use it as an effective PDT tool. The PS molecules can be easily adsorbed onto the NPs via the swelling diffusion technique. This places the upconverting NPs and PS molecules close to each other for the effective production of $^1O_2$. Recently, our group has synthesized upconverting hydrogel nanocomposites using a simple thiol−ene click reaction and used them as a template for the synthesis of dendrimer-like Au nanostructures.[52]

In this work, we have synthesized Ln^{3+}-doped upconverting hydrogel nanocomposite and evaluated its potential for photodynamic therapy. The nanocomposite was prepared by first synthesizing the 10-undecenoic acid (10-UDA)-capped Yb^{3+}/Er^{3+}-doped $NaYF_4$ NPs via a microwave procedure. The carboxylic group at one terminal attaches to the NP surface, whereas the double bond present at the surface of the NPs is used to react with monomer *N*-isopropylacrylamide (NIPAM) and cross-linker methylene bisacrylamide (MBA) with azobisisobutyronitrile (AIBN) as a thermal initiator to form a hydrogel composite. The hydrogel nanocomposites displayed strong NIR-to-visible (500−700 nm) upconversion emission under the excitation from the 980 nm laser. The emission near 650 nm was used to activate the MB for the generation of singlet oxygen, as its absorption maxima match well with the 650 nm emission of the upconverting NPs. The MB molecules were easily loaded onto the upconverting hydrogel nanocomposites because of the highly porous nature, and a high swelling ratio of composite gels in water was observed. These hydrogel nanocomposites can reduce the distance between MB and upconverting NPs as well as effectively protect the MB dye from the denaturation instigated by the extreme environment. The results suggest that the (NIPAM-MBA@UDA-$NaYF_4:Yb^{3+}/Er^{3+}$)@MB hydrogel nanocomposite can be used as carriers for PS methylene blue dye in the PDT.

RESULTS AND DISCUSSIONS

The upconverting NPs were synthesized using the microwave irradiation-assisted technique. The phase purity and crystallinity of the NPs were analyzed by the powder X-ray diffraction (PXRD) analyses. Figure 1a shows the PXRD pattern of the

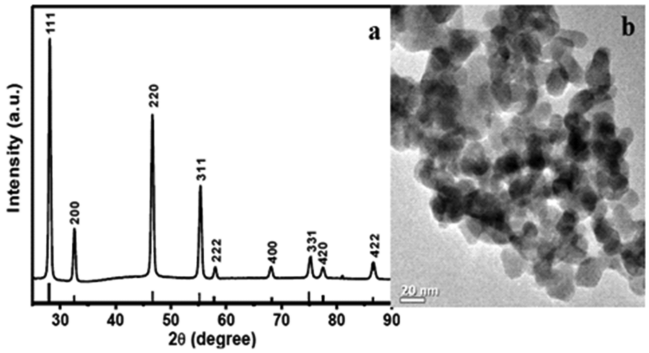

Figure 1. (a) PXRD pattern and (b) TEM image of 10-undecenoic acid (10-UDA)-capped Yb^{3+}/Er^{3+}-doped $NaYF_4$ NPs. The vertical lines in (a) are the standard pattern of cubic phase bulk $NaYF_4$.

10-UDA-capped Yb^{3+}/Er^{3+}-doped $NaYF_4$ NPs. From the figure, it is clear that the NPs formed are cubic phase (α) $NaYF_4$ (JCPDF 06-0432) as the peak positions and intensities of the NPs matched well to the standard of bulk. The PXRD peaks clearly suggested the formation of the highly crystalline nature of the NPs synthesized. The size and morphology analysis was performed using transmission electron microscopy (TEM) as shown in Figure 1b. The TEM image of the 10-UDA-capped Yb^{3+}/Er^{3+}-doped $NaYF_4$ NPs shows that the particles were aggregated with a distorted spherical nature. The average size of the NPs was close to 20 nm. The high-resolution TEM (HRTEM) image confirms the highly crystalline nature of the synthesized NPs with an interplaner distance of 0.326 nm corresponding to the (111) plane and 0.199 nm corresponding to the (220) plane of α-phase $NaYF_4$ NPs, as shown in Figure S1a. The selected area electron diffraction (SAED) pattern also confirms the presence of major peaks present in the crystalline cubic phase of $NaYF_4$ NP. The SAED pattern of the NPs is shown in Figure S1b. We believe that the aggregation of the NPs is due to the weak interaction between the double bonds of the neighboring NPs (vide infra). The NPs were highly dispersible in dimethylsulphoxide (DMSO) which is a polar organic solvent. The high dispersibility of the NPs in DMSO suggests the strong attachment of 10-UDA to the surface of the NPs.

The elemental composition was confirmed from elemental mapping followed by line scanning which confirmed the presence of sodium, yttrium, ytterbium, erbium, and fluoride atoms as shown in Figures S2 and S3. Also, the energy-dispersive X-ray spectroscopy (EDX) spectrum showed the presence of the abovementioned elements (see Figure S4).

DOI: 10.1021/acsomega.8b02416
ACS Omega 2019, 4, 3169−3177

The surface functionalization of the NPs with 10-UDA molecules was determined by using Fourier transform infrared spectroscopy (FTIR). Figure 2 shows the FTIR spectra of pure

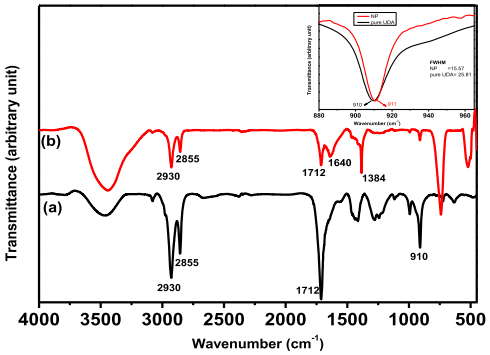

Figure 2. FTIR spectra of (a) pure 10-UDA- and (b) 10-UDA-capped Yb^{3+}/Er^{3+}-doped $NaYF_4$ NPs. The inset shows the expanded view of the C═C−H bending region along with fwhm of the corresponding peaks.

10-UDA and 10-UDA-capped NPs. The peak observed near 1712 cm^{-1} corresponds to C═O stretching vibration of the COOH group present in pure 10-UDA. The C═O stretching vibration is shifted to 1640 cm^{-1} with reduced peak intensity upon binding to the NP surface. The sharp bands appearing near 2855 and 2930 cm^{-1} are due to the symmetric and asymmetric CH_2 stretching vibration modes, respectively, in 10-UDA, which are also observed for the 10-UDA-capped NPs. Another small peak is observed at 3080 cm^{-1} belonging to the C−H stretching of the HC═CH_2 group, which is present in both pure 10-UDA as well as in 10-UDA-capped Yb^{3+}/Er^{3+}-doped $NaYF_4$ NPs. We tried to get more details regarding the aggregation of NPs observed in the TEM image from the FTIR results, as it will be more sensitive to changes in the C═C−H vibrational frequencies. Because of the overlap of the −C═C−H stretching frequency (~1640 cm^{-1}) with the carbonyl stretching frequency of $-COO^-$ groups in the NPs, we tried to compare the −C═C−H bending vibration at 910 cm^{-1}. Though there is only a slight shift toward higher energy, the peak broadening is quite different. The full width at half-maximum (fwhm) of the peak shifts from 25.57 to 15.81 for the NP (see inset of Figure 2). This may be likely due to interactions between the double bonds resulting in longer relaxation time for the bending vibration.

The UC NPs are known for their characteristic optical pattern of showing the anti-Stokes emission by converting low-energy photons into high-energy photons (in this case, Yb^{3+}/Er^{3+}-doped $NaYF_4$ NPs can convert NIR light of 980 nm into visible light in the green and red region). The luminescence behavior of the UC NPs was studied using a 980 nm diode laser. Figure 3 shows the upconversion emission spectrum of the UDA-capped Yb^{3+}/Er^{3+}-doped $NaYF_4$ NPs in DMSO for 0.1% (wt/vol) of NP dispersion. Upon 980 nm excitation, the Yb^{3+}/Er^{3+}-doped $NaYF_4$ NPs display three emission bands centered at 521, 540, and 650 nm. These emission bands are respectively assigned to $^2H_{11/2} \rightarrow {}^4I_{15/2}$, $^4S_{3/2} \rightarrow {}^4I_{15/2}$, and $^4F_{9/2} \rightarrow {}^4I_{15/2}$ transitions of the excited Er^{3+} ions. The upconversion emission spectrum observed is due to two-photon energy transfer from excited Yb^{3+} ions to the Er^{3+} ions. Yb^{3+} ions have a high absorption coefficient around 980 nm, it acts as a sensitizer for the Er^{3+} ions which are the activator

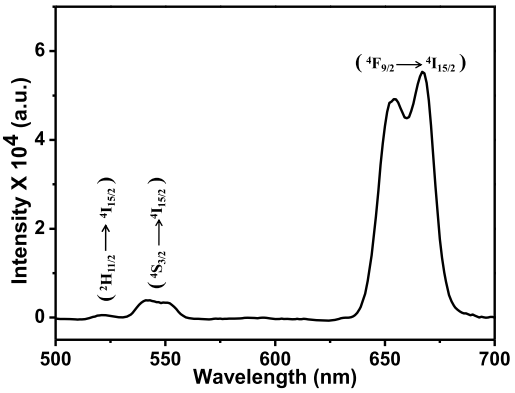

Figure 3. Upconversion emission spectrum of the 10-UDA-capped Yb^{3+}/Er^{3+}-doped $NaYF_4$ NPs in DMSO (0.5 wt %).

ions. The upconversion mechanism is similar to the previously reported mechanism.[53−55]

The UC NPs were transferred into gel-based composites for them to be used in PDT. Our idea was to use the UC NPs in the hydrogel form for efficient PDT. For this purpose, the UC NPs were incorporated into a gel-based matrix as a nanocomposite. The double bond present at the surface of the NPs were utilized in the synthesis of nanocomposite gels. 10-UDA-capped Yb^{3+}/Er^{3+}-doped $NaYF_4$ NPs were converted into a gel form by the addition of NIPAM and *N*,*N*-methylenebis(acrylamide) (MBA) solutions in the presence of thermal radical initiator AIBN. NIPAM and MBA are the monomer and cross-linking agent, respectively. These molecules have the ability to form cross-linked networks with the double bond moiety present on the surface of the Yb^{3+}/Er^{3+}-doped $NaYF_4$ NPs. The gel formation was completed within 15 min with continuous stirring at 70 °C under an Ar atmosphere. After 15 min, the synthesized gel was sticking to the bottom of the reaction flask. Also, the rotation of the magnetic stirrer was reduced which was proof that the gelation has occurred. The purification of the gel was performed by washing the gel with DMSO for 5 times. Scheme 1 shows the schematic representation of the synthesis of NIPAM-MBA@10-UDA-$NaYF_4$:Yb^{3+}/Er^{3+} gel and the inset shows the digital image of the gel formed inside the cuvette.

The phase of the NPs after gel formation was confirmed by the PXRD analysis. The PXRD pattern of NPs after gel formation is shown in Figure S5. The X-ray diffraction pattern matches well with the UDA-capped Yb^{3+}/Er^{3+}-doped $NaYF_4$ NPs confirming that the phase of the NPs is well preserved and not affected after gel formation. To understand the morphology of the resulting nanocomposite gels, scanning electron microscopy (SEM) analysis was performed. The 10-UDA-capped NPs after gel formation resulted in nonporous fiber-like architecture. Figure 4 shows the SEM images of the resulting (NIPAM-MBA-10-UDA@$NaYF_4$:Yb^{3+}/Er^{3+}) gel.

The nanocomposite gel was further characterized with FTIR analysis. Figure S6 shows the FTIR spectrum of Yb^{3+}/Er^{3+}-doped $NaYF_4$ composite gel. The C−H stretching of the HC═CH_2 group, which appeared at 3080 cm^{-1} for the UDA-capped Yb^{3+}/Er^{3+}-doped $NaYF_4$ NPs, is absent in the spectrum of the composite gel. It suggests that the NPs are covalently bound to the NIPAM and MBA. A distinct carbonyl stretching signal observed at 1648 cm^{-1} confirms the presence of C═O stretching of the −CONH−group in the gel.

DOI: 10.1021/acsomega.8b02416
ACS Omega 2019, 4, 3169−3177

Scheme 1. Schematic Representation of the Synthesis of NIPAM-MBA@UDA-$NaYF_4$:Yb^{3+}/Er^{3+} Nanocomposite Gels[a]

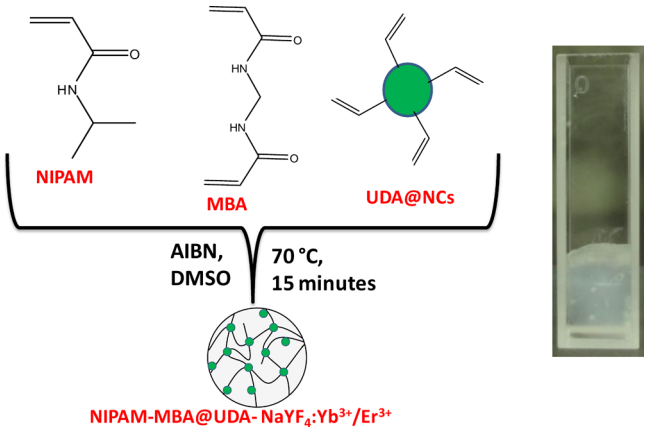

[a]The inset shows the upconverting gel in the cuvette.

The structure and crystalline behavior of the formed hydrogel were confirmed using TEM, HRTEM, and SAED patterns as shown in Figures S7 and S8. The nanocomposite has irregular morphology as was the case of 10-UDA-capped NPs. In case of hydrogel, it is confirmed that the NPs are closely spaced from each other because of the hydrogel formed surrounding it. The interplaner spacing of 0.332 nm corresponding to the (111) plane is the same as cubic-phased $NaYF_4$ NP which again confirms the presence of NPs inside the hydrogel. The SAED pattern also shows the formation of two concentric rings only corresponding to the highest intensity peaks present in cubic-phase $NaYF_4$ NPs. The elemental composition has been confirmed by mapping and line scanning as shown in Figures S9 and S10.

The luminescence behavior of the upconverting composite gel of the Yb^{3+}/Er^{3+}-doped $NaYF_4$ NPs was retained even after gel formation. Figure 5 shows the upconversion luminescence spectra of NPs before and after gel formation. Interestingly, the UC emission spectra clearly show that the intensity of upconversion luminescence for gel composites increased upto 4 times compared to UDA-capped Yb^{3+}/Er^{3+}-doped $NaYF_4$ NPs. In order to confirm the increase in emission of the Er^{3+} ion, lifetime decay analysis was carried out using direct excitation at 485 nm observing both the 540 nm ($^4S_{3/2} \rightarrow {}^4I_{15/2}$) and 650 nm ($^4F_{9/2} \rightarrow {}^4I_{15/2}$). As shown in Figures S11 and S12, the lifetime of the 540 nm emission increased to 202.2 μs from 141.62 μs, whereas the values of the red emission increased to 157.15 from 140.18 μs upon gel

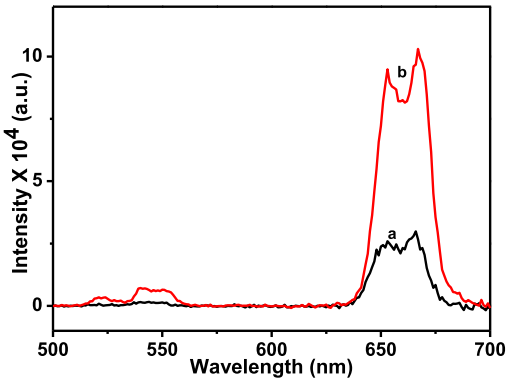

Figure 5. Upconversion emission spectra of (a) UDA-capped Yb^{3+}/Er^{3+}-doped $NaYF_4$ NPs and (b) after gel formation (both measured in solid state under identical conditions).

formation. This is clearly in accordance with the enhancement of emission intensity of the hydrogel sample as compared to 10-UDA-capped $NaYF_4$ NPs. We presume that this may be due to reduction in the defects at the surface or less quenching from the solvent, thereby reducing the rate of nonradiative decay. This results in the increase in the intensity of the Er^{3+} emissions.

We noted that the gel nanocomposite was barely dispersible in any nonpolar or aprotic solvent. We believe that because of the cross-linking network of the UDA-capped Yb^{3+}/Er^{3+}-doped $NaYF_4$ NPs with NIPAM and MBA, the dispersibility of the composite gels was very low in nonpolar and aprotic polar solvents. The above results evidently indicated the formation of the composite gels.

The swelling behavior of the upconverting nanocomposite gel was studied by carrying out swelling measurements on the resulting nonporous composite gels in polar and nonpolar solvents such as water and toluene, respectively. Figure 6 shows the SEM images of the composite gels after being exposed to water and toluene. The composite gels in water show the aggregation of fibers with pores in it. The same gel nanocomposite in toluene shows the presence of fibers without pores, suggesting that the swelling behavior of gels is achieved in the presence of water. The selective swelling in water implies that the developed composite gels are hydrogels which can absorb water because of formation of hydrogen bonding. Nearly 200% (by weight) swelling was observed for composite gels in water within 1 h duration. The observed swelling behavior was attributed to the presence of water molecules and several hydrophilic sites in the nanocomposite gels, allowing electrostatic repulsion due to the formation hydrogen bonding interaction.

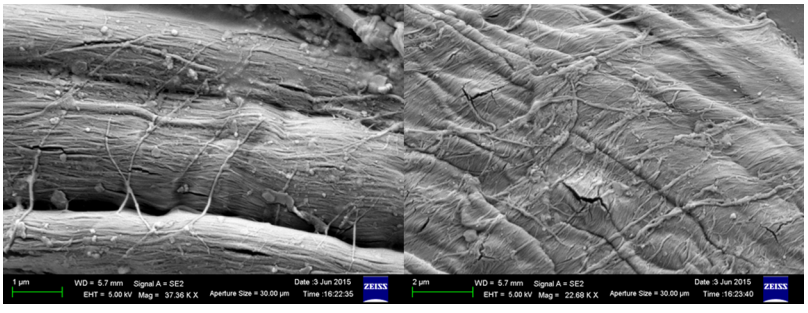

Figure 4. SEM images of the upconverting nanocomposite gel (NIPAM-MBA@UDA-$NaYF_4$:Yb^{3+}/Er^{3+}).

DOI: 10.1021/acsomega.8b02416
ACS Omega 2019, 4, 3169−3177

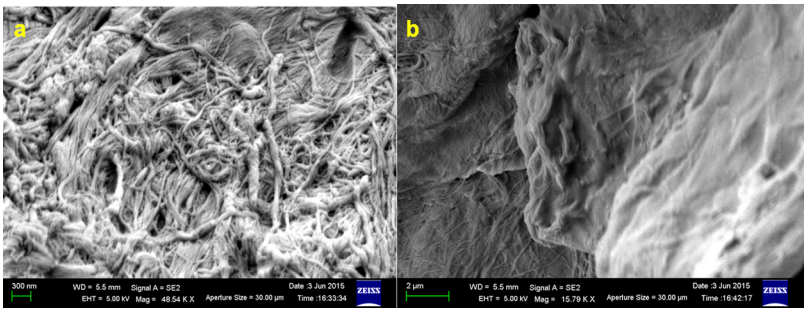

Figure 6. SEM images of upconverting nanocomposite gel in (a) water and (b) toluene.

To utilize the upconverting hydrogel nanocomposites for NIR-laser-triggered PDT, MB was chosen as a model PS because of its high quantum yield of $^1O_2$ generation (0.5),[56] negligible dark toxicity, and its hydrophilic nature. Moreover, the absorption of methylene blue matches well with the red UC emission of Er^{3+} ions. Figure 7 clearly shows the spectral

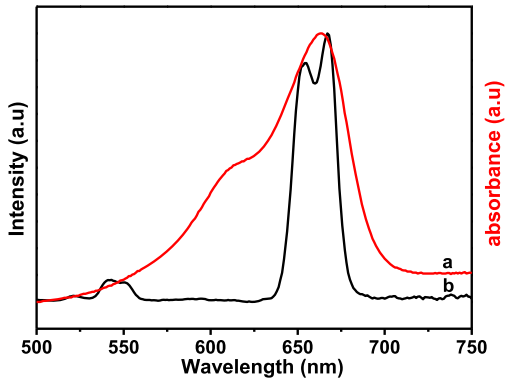

Figure 7. Overlap between MB absorption and $NaYF_4$:Yb^{3+}/Er^{3+} emission spectra. (a) UV/vis absorption spectrum of MB in water and (b) emission spectrum of $NaYF_4$:Yb^{3+}/Er^{3+} NPs under NIR-laser excitation.

overlap between absorption (654 nm) of MB and red emission (651 nm) of 10-UDA-capped Yb^{3+}/Er^{3+}-doped $NaYF_4$ NPs. This high spectral overlap suggests possibility of efficient energy transfer between the activator molecules Er^{3+} to the PS MB.

Loading of MB. The hydrophilic nature of the gel along with its porous nature and large swelling behavior were ideal for the high loading capacity of MB into the upconverting nanocomposite gel. The loading of MB onto the NIPAM-MBA@UDA-$NaYF_4$:Yb^{3+}/Er^{3+} hydrogel was performed by a simple swelling-diffusion technique. Because of the high swelling ability of the hydrogel nanocomposite in water, the loading of MB was easy onto the NIPAM-MBA@10-UDA-$NaYF_4$:Yb^{3+}/Er^{3+} hydrogel. Briefly, 3 mL of 0.01 mM MB was added to a small piece of the (NIPAM-MBA@10-UDA-$NaYF_4$:Yb^{3+}/Er^{3+}) hydrogel composite for 1 h at room temperature. Free MB molecules were removed by re-dispersing the MB-loaded upconverting hydrogel nanocomposite in water for 30 min and removing the supernatant. This procedure was repeated 3 times. The resulting (NIPAM-MBA@10-UDA-$NaYF_4$:Yb^{3+}/Er^{3+})@MB hydrogel nanocomposite was colored, indicating the successful loading of MB within the upconverting hydrogel matrix. This was further confirmed by UV−vis absorption studies. Figure 8 shows UV−

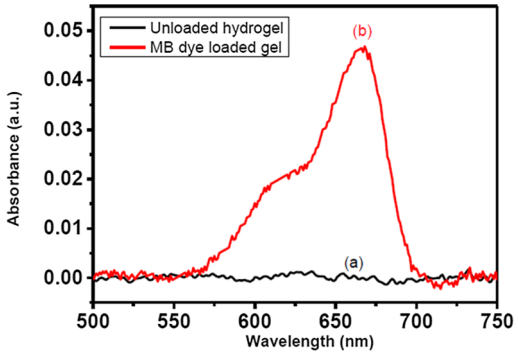

Figure 8. UV−visible absorption spectra of (a) (NIPAM-MBA@UDA-$NaYF_4$:Yb^{3+}/Er^{3+}) hydrogel and (b) (NIPAM-MBA@UDA-$NaYF_4$:Yb^{3+}/Er^{3+})@MB.

vis spectra of MB dye-loaded nanocomposite gel along with the gel without MB. A strong absorption peak characteristic of MB is observed near 654 nm for the gel, whereas barely any absorption was noted for the gel (without MB) Figure 8. As quantitative estimation of the PS (MB) loading into the gel is difficult to calculate directly from the UV−vis absorbance measurements of the gel samples, we used an indirect method. The loading efficiency was determined by calculating the change in the characteristic absorption peak of MB before and after loading to the hydrogel nanocomposite. The calculated value is about 78% for 1 h loading (Figure S13 in Supporting Information). A decrease in absorbance of the supernatant dye solution after 1 h is caused because of adsorption of the dye solution in the porous network of the hydrogel (see Figure S13). The PS loading efficiency is about 78% calculated using the difference in the absorbance.

To understand the change in the luminescence properties of (NIPAM-MBA@10-UDA-$NaYF_4$:Yb^{3+}/Er^{3+}) nanocomposites after MB loading onto the hydrogel composite, the luminescence measurements were performed. Figure 9 shows the comparison of the upconversion emission spectra of (NIPAM-MBA@10-UDA-$NaYF_4$:Yb^{3+}/Er^{3+}) hydrogel and MB-loaded upconverting hydrogel. It is quite clear that the intensity of the red emission is greatly reduced for MB-loaded upconverting hydrogel. The calculated red to green (R/G) ratio was found to be 5.71 for upconverting hydrogel and this value reduced to 0.51 for the MB-loaded upconverting hydrogel. The significant quenching in the intensity of the red emission of (NIPAM-MBA@UDA $NaYF_4$:Yb^{3+}/Er^{3+})@MB indicates the direct evidence of energy transfer from upconverting NPs to MB. This is reasonable because of the overlap between the red emission of the upconverting NPs and the absorption of MB (see Figure 7).

DOI: 10.1021/acsomega.8b02416
ACS Omega 2019, 4, 3169−3177

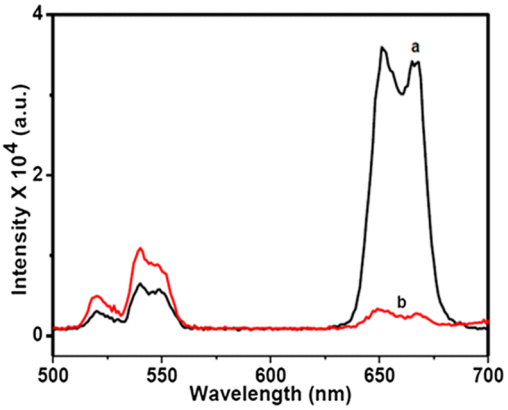

Figure 9. Upconversion emission spectra of (a) hydrogel nanocomposite (NIPAM-MBA@10-UDA-$NaYF_4$:Yb^{3+}/Er^{3+}) and (b) MB-loaded hydrogel composite (NIPAM-MBA@10-UDA-$NaYF_4$:Yb^{3+}/Er^{3+})@MB.

Determination of Singlet Oxygen. To estimate ROS-like singlet oxygen production from (NIPAM-MBA@10-UDA-$NaYF_4$:Yb^{3+}/Er^{3+})@MB hydrogel composite upon NIR irradiation, 1,3-diphenylisobenzofuran (DPBF), a widely used singlet oxygen quencher was used in our experiment. Singlet oxygen production was inversely proportional to the intensity of the DPBF photoluminescence (PL) band at 485 nm when excited at 365 nm. 15 μL of DPBF in acetonitrile was added to a small piece of (NIPAM-MBA@10-UDA-$NaYF_4$:Yb^{3+}/Er^{3+})@MB composite gel and exposed to NIR light (980 nm with 500 mW power) for 30 min. A rapid decrease in the intensity of the DPBF PL band at 485 nm is observed for the (NIPAM-MBA@10-UDA-$NaYF_4$:Yb^{3+}/Er^{3+})@MB hydrogel (25% within 10 min). A 50% reduction in the PL intensity was noted after 30 min of NIR laser irradiation (Figure 10). This

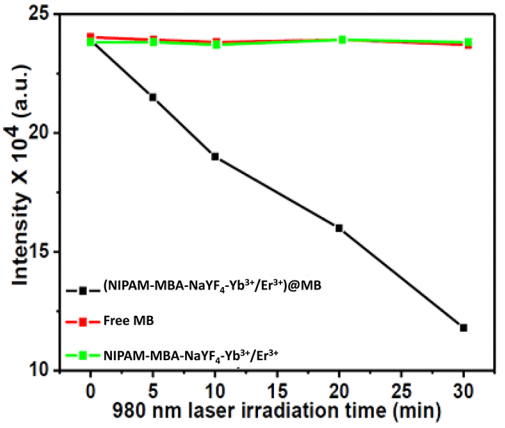

Figure 10. Plot of DPBF emission (480 nm) intensity versus laser irradiation time [the singlet-oxygen generation under NIR-laser irradiation (λ = 980 nm)].

demonstrates the increase in the generation of singlet oxygen with the irradiation time. The result indicates that most of the MB in the excited state might transfer their energy to surrounding oxygen upon irradiation by NIR light. To confirm that the singlet oxygen produced by MB via excitation of the upconverting NPs, two control experiments were performed. First, a mixture of free MB molecules and DPBF in acetonitrile was prepared and exposed to a 980 nm laser. Second, a mixture of (NIPAM-MBA@10-UDA-$NaYF_4$:Yb^{3+}/Er^{3+}) hydrogel containing the DPBF prepared in acetonitrile was exposed to 980 nm laser light (without MB). The resulting mixtures were excited at 365 nm to observe the peak at 485 nm. Both the control experiments suggest that there is no change in the intensity of the PL band at 485 nm (shown in Figure 10). These results imply that MB was effectively activated by the emission from upconverting NPs which led to the production of singlet oxygen.

CONCLUSIONS

In conclusion, an upconverting hydrogel nanocomposite (NIPAM-MBA-10-UDA@$NaYF_4$:Yb^{3+}/Er^{3+}) was synthesized by reacting the UDA-capped Yb^{3+}/Er^{3+}-doped $NaYF_4$ NPs with a thermosensitive NIPAM monomer using the thermal initiator AIBN. The PS (MB) was efficiently confined in a NIPAM hydrogel matrix to form (NIPAM-MBA@10-UDA-$NaYF_4$:Yb^{3+}/Er^{3+})@MB using a swelling diffusion method. The hydrogel nanocomposites display high swelling characteristics in water, resulting in porous structures leading to high loading of MB (~78% in 1 h). The MB-loaded upconverting hydrogel nanocomposites have been evaluated for their application in NIR-laser-triggered PDT. The experimental results have shown that the emission from upconverting NPs excited by NIR radiation can effectively activate the PS (MB) to generate ROS such as singlet oxygens. The results suggest that the developed composite gel can find potential use in PDT.

EXPERIMENTAL SECTION

Materials. Y_2O_3, Yb_2O_3, Er_2O_3, CF_3COONa, 10-UDA, 1-octadecene (90%), $CDCl_3$, DPBF, NIPAM, MBA, and AIBN were purchased from Sigma-Aldrich. Ethanol, dichloromethane, DMSO, trifluoroacetic acid, toluene, hexane, were purchased from Merck. All chemicals were used without further purification.

Synthesis of UDA Capped Yb^{3+}/Er^{3+}-Doped $NaYF_4$ NPs. A commercial microwave reactor (ANTONPAR) system was used for the synthesis of the 10-UDA-capped Yb^{3+}/Er^{3+}-doped $NaYF_4$ NPs. In a typical procedure, the mixture of 0.78 mmol of $Y(NO_3)_3$, 0.20 mmol of $Yb(NO_3)_3$, and 0.02 mmol of $Er(NO_3)_3$ were added to 10 mL distilled water in a 50 mL round-bottom flask. Then, 2 mmol of 10-UDA in 5 mL ethanol was added to the reaction mixture and stirred for 2 h. Subsequently, 8 mmol of NaF in 10 mL water was added to the above mixture and stirred for 1 h. Subsequently, the mixture of nitrate solution in a capping agent with the fluoride solution was transferred to a microwave reaction vessel. The resultant reaction mixture was heated to 160 °C for 10 min with eventual cooling to room temperature. The mixture was precipitated by the addition of ethanol and isolated by centrifugation at 3600 rpm for 10 min. The isolated 10-UDA-capped Yb^{3+}/Er^{3+}-doped $NaYF_4$ NPs were dried under vacuum for 24 h.

Synthesis of (NIPAM-MBA@UDA-$NaYF_4$:Yb^{3+}/Er^{3+}) Hydrogel. In a typical reaction, 3.4 mmol NIPAM and 0.075 mmol MBA were added to a flask containing 1.5 mL DMSO and sonicated for 10 min or until the solution turns to clear. Then, 20 mg of 10-UDA capped Yb^{3+}/Er^{3+}-doped $NaYF_4$ NPs in 1 mL DMSO and 5 mg AIBN were added to the above mixture. The mixture was stirred with a magnetic stirrer at 25 °C under Ar atmosphere for 15 min. The resulting mixture was slowly heated to 70 °C under an Ar atmosphere and

DOI: 10.1021/acsomega.8b02416
ACS Omega 2019, 4, 3169−3177

maintained for 15 min at this temperature. The (NIPAM-MBA-10-UDA-$NaYF_4$:Yb^{3+}/Er^{3+}) hydrogel nanocomposites was purified by removing the byproducts and by dispersing in DMSO. The hydrogel nanocomposites were dried under vacuum at 60 °C.

Swelling Study of (NIPAM-MBA@10-UDA-$NaYF_4$:Yb^{3+}/Er^{3+}) Hydrogel Nanocomposites. A preweighed sample of the (NIPAM-MBA@10-UDA-$NaYF_4$:Yb^{3+}/Er^{3+}) hydrogel nanocomposite was kept in a 20 mL glass vial and dispersed in 10 mL of distilled water. At regular intervals, the nanocomposite gel was taken out of the glass vial using forceps and weighed after blotting on an absorbent tissue paper to eliminate excess solvent water molecules. The water uptake was calculated using the following equation

$$W_{up} = 100 \times (W_{wet} - W_{dry})/W_{dry}$$

W_{up} refers to the water uptake, and W_{wet} and W_{dry} refer to the weight of wet and dry nanocomposite gel, respectively. Swelling experiments were repeated 3 times for upconverting hydrogel nanocomposites. A similar study was performed for the swelling measurements in hexane.

Loading of MB onto (NIPAM-MBA@10-UDA-$NaYF_4$:Yb^{3+}/Er^{3+}) Hydrogel Nanocomposites. Before the addition of MB to the hydrogel nanocomposites, the absorbance of MB was recorded at 660 nm using a UV−visible spectrometer. The loading of MB onto the (NIPAM-MBA@10-UDA-$NaYF_4$:Yb^{3+}/Er^{3+}) hydrogel nanocomposites was carried out by adding 3 mL of 10 μM MB to the small piece of (NIPAM-MBA@10-UDA-$NaYF_4$:Yb^{3+}/Er^{3+}) hydrogel nanocomposites for 1 h at room temperature. Free MB molecules were removed by re-dispersing the upconverting hydrogel nanocomposites in water and removed supernatants 3 times. Finally, the absorbance of the supernatant was measured at 660 nm. The resulting (NIPAM-MBA@10-UDA-$NaYF_4$:Yb^{3+}/Er^{3+})@MB composite was dried for further use. The percentage of MB loaded into the hydrogel nanocomposites was calculated from the following equation

methylene blue loading (%) = (methylene blue dye solution added − methylene blue dye present in supernatant) /methylene blue added × 100

Singlet Oxygen ($^1O_2$) Detection. DPBF was used as a probe to detect the singlet oxygen ($^1O_2$) through luminescent measurements. In a typical experiment, 30 μL of DPBF in acetonitrile (5.0 mM) was mixed with 50 mg of the (NIPAM-MBA@10-UDA-$NaYF_4$:Yb^{3+}/Er^{3+})@MB composite in 2 mL acetonitrile. Free MB molecules or 10-UDA-capped Yb^{3+}/Er^{3+}-doped $NaYF_4$ NPs (bare NPs) were dispersed in acetonitrile solvent and mixed with DPBF which was used for the control experiments The solutions were constantly irradiated by 980 nm NIR laser and emission at 485 nm was observed at fixed time intervals. The $^1O_2$ generated by photoexcitation of MB dye solution reacts irreversibly with DPBF, thus decreasing the intensity of the DPBF PL band at 485 nm when excited at 365 nm.

Characterization. The PXRD patterns of the 10-UDA-capped NPs were acquired using a Rigaku-SmartLab X-ray diffractometer with a D/tex Ultradetector and a Cu Kα source operating at 40 kV and 50 mA. The scan range was set from 20° to 90° with a step size of 0.020 and scan rate of 2°/min. The samples were powdered completely and spread evenly on a quartz slide. Field-emission SEM images were collected on the SUPRA 55-VP JSM-with patented GEMINI column technology. The samples loaded into the instrument were first coated with a thin film of gold in order to avoid charging effects. Samples were prepared by placing a drop of dilute DMSO/H_2O/toluene dispersion of NPs and hydrogel nanocomposites. The size and morphology of the NPs were obtained using the FEI Tecnai G2 UTwin (200 keV) TEM instrument. The mapping and SAED pattern analyses were also carried out using the same instrument. The absorption measurements were recorded using a Hitachi U4100 spectrophotometer. The samples were taken in a 3 mL quartz cuvette (path length, 1 cm). FTIR spectra were acquired with a PerkinElmer FTIR spectrometer 1000 with a resolution of 2 cm^{-1}. The solid samples were taken as dry powder and pelletized with KBr, and the pellets were placed on the sample holder. Upconversion measurements were done by exciting the 1 wt % NP dispersion with a 980 nm diode laser from RgBLase LLC, which was coupled to a fiber with a core diameter of 100 μm. The emitted light was detected using a Horiba JobinYvon fluorimeter equipped with a photomultiplier tube. To remove the scattered excitation light, a long-band pass filter (495 nm) was used on the excitation side. All upconversion emission spectra were measured with the same slit width at the same excitation laser power of 500 mW.

■ ASSOCIATED CONTENT

Supporting Information

The Supporting Information is available free of charge on the ACS Publications website at DOI: 10.1021/acsomega.8b02416.

TEM images, SAED, and EDX results of NPs and composites, lifetime decay curves, PXRD and FTIR spectra of nanocomposites (PDF)

■ AUTHOR INFORMATION

Corresponding Author

*E-mail: mvenkataramanan@yahoo.com (V.M.).

ORCID

Venkataramanan Mahalingam: 0000-0003-1414-805X

Notes

The authors declare no competing financial interest.

■ ACKNOWLEDGMENTS

V.M. thanks CSIR for the project (SR/S1/IC-46/2010), DST and Indian Institute of Science Education and Research (IISER), Kolkata for the funding. B.M. and D.S. thank the IISER Kolkata for funding.

■ REFERENCES

(1) Dougherty, T. J.; Gomer, C. J.; Henderson, B. W.; Jori, G.; Kessel, D.; Korbelik, M.; Moan, J.; Peng, Q. Photodynamic Therapy. *J. Natl. Cancer Inst.* **1998**, *90*, 889−905.

(2) Croissant, J. G.; Picard, S.; Aggad, D.; Klausen, M.; Mauriello Jimenez, C.; Maynadier, M.; Mongin, O.; Clermont, G.; Genin, E.; Cattoën, X.; Wong Chi Man, M.; Raehm, L.; Garcia, M.; Gary-Bobo, M.; Blanchard-Desce, M.; Durand, J.-O. Fluorescent periodic mesoporous organosilica nanoparticles dual-functionalized via click chemistry for two-photon photodynamic therapy in cells. *J. Mater. Chem. B* **2016**, *4*, 5567−5574.

(3) Brown, S. B.; Brown, E. A.; Walker, I. The present and future role of photodynamic therapy in cancer treatment. *Lancet Oncol.* **2004**, *5*, 497−508.

DOI: 10.1021/acsomega.8b02416
ACS Omega 2019, 4, 3169−3177

(4) Zhu, X.; Wang, H.; Zheng, L.; Zhong, Z.; Li, X.; Zhao, J.; Kou, J.; Jiang, Y.; Zheng, X.; Liu, Z.; Li, H.; Cao, W.; Tian, Y.; Wang, Y.; Yang, L. Upconversion nanoparticle-mediated photodynamic therapy induces THP-1 macrophage apoptosis via ROS bursts and activation of the mitochondrial caspase pathway. *Int. J. Nanomed.* **2015**, *10*, 3719−3736.
(5) Chatterjee, D. K.; Fong, L. S.; Zhang, Y. Nanoparticles in photodynamic therapy: an emerging paradigm. *Adv. Drug Delivery Rev.* **2008**, *60*, 1627−1637.
(6) Dolmans, D. E. J. G. J.; Fukumura, D.; Jain, R. K. Photodynamic Therapy for Cancer. *Nat. Rev. Cancer* **2003**, *3*, 380−387.
(7) Lovell, J. F.; Liu, T. W. B.; Chen, J.; Zheng, G. Activatable photosensitizers for imaging and therapy. *Chem. Rev.* **2010**, *110*, 2839−2857.
(8) Macdonald, I. J.; Dougherty, T. J. Basic Principles of Photodynamic Therapy. *J. Porphyrins Phthalocyanines* **2001**, *5*, 105−129.
(9) Wang, C.; Tao, H.; Cheng, L.; Liu, Z. Near-infrared light induced in vivo photodynamic therapy of cancer based on upconversion nanoparticles. *Biomaterials* **2011**, *32*, 6145−6154.
(10) Spyratou, E.; Makropoulou, M.; Mourelatou, E. A.; Demetzos, C. Biophotonic techniques for manipulation and characterization of drug delivery nanosystems in cancer therapy. *Cancer Lett.* **2012**, *327*, 111−122.
(11) Hemmer, E.; Venkatachalam, N.; Hyodo, H.; Hattori, A.; Ebina, Y.; Kishimoto, H.; Soga, K. Upconverting and NIR emitting rare earth based nanostructures for NIR-bioimaging. *Nanoscale* **2013**, *5*, 11339−11361.
(12) Auzel, F. Upconversion and anti-stokes processes with f and d ions in solids. *Chem. Rev.* **2004**, *104*, 139−174.
(13) Haase, M.; Schäfer, H. Upconverting nanoparticles. *Angew. Chem., Int. Ed.* **2011**, *50*, 5808−5829.
(14) Wang, F.; Han, Y.; Lim, C. S.; Lu, Y.; Wang, J.; Xu, J.; Chen, H.; Zhang, C.; Hong, M.; Liu, X. Simultaneous phase and size control of upconversion nanocrystals through lanthanide doping. *Nature* **2010**, *463*, 1061−1065.
(15) Wang, J.; Wang, F.; Wang, C.; Liu, Z.; Liu, X. Single-band upconversion emission in lanthanide-doped $KMnF_3$ nanocrystals. *Angew. Chem., Int. Ed.* **2011**, *50*, 10369−10372.
(16) Johnson, N. J. J.; Sangeetha, N. M.; Boyer, J.-C.; van Veggel, F. C. J. M. Facile ligand-exchange with polyvinylpyrrolidone and subsequent silica coating of hydrophobic upconverting β-$NaYF_4$:Yb^{3+}/Er^{3+} nanoparticles. *Nanoscale* **2010**, *2*, 771−777.
(17) Sarkar, S.; Meesaragandla, B.; Hazra, C.; Mahalingam, V. Sub-5 nm Ln^{3+}-doped $BaLuF_5$ nanocrystals: a platform to realize upconversion via interparticle energy transfer (IPET). *Adv. Mater.* **2012**, *25*, 856−860.
(18) Eliseeva, S. V.; Bünzli, J.-C. G. Lanthanide luminescence for functional materials and bio-sciences. *Chem. Soc. Rev.* **2010**, *39*, 189−227.
(19) Meesaragandla, B.; Adusumalli, V. N. K. B.; Mahalingam, V. Methyl oleate-capped upconverting nanocrystals: a simple and general ligand exchange strategy to render nanocrystals dispersible in aqueous and organic medium. *Langmuir* **2015**, *31*, 5521−5528.
(20) Schäfer, H.; Ptacek, P.; Zerzouf, O.; Haase, M. Synthesis and optical properties of KYF_4/Yb, Er nanocrystals, and their surface modification with undoped KYF_4. *Adv. Funct. Mater.* **2008**, *18*, 2913−2918.
(21) Kumar, K. U.; Linganna, K.; Babu, S. S.; Piccinelli, F.; Speghini, A.; Giarola, M.; Mariotto, G.; Jayasankar, C. K. Synthesis, structural properties and upconversion emission of Er^{3+} and Er^{3+}/Yb^{3+} doped nanocrystalline $NaNbO_3$. *Sci. Adv. Mater.* **2012**, *4*, 1−7.
(22) Ximendes, E. C.; Santos, W. Q.; Rocha, U.; Kagola, U. K.; Sanz-Rodríguez, F.; Fernández, N.; Gouveia-Neto, A. d. S.; Bravo, D.; Domingo, A. M.; del Rosal, B.; Brites, C. D. S.; Carlos, L. D.; Jaque, D.; Jacinto, C. Unveiling in vivo subcutaneous thermal dynamics by infrared luminescent nanothermometers. *Nano Lett.* **2016**, *16*, 1695−1703.
(23) Quintanilla, M.; Cantarelli, I. X.; Pedroni, M.; Speghini, A.; Vetrone, F. Intense ultraviolet upconversion in water dispersible SrF2:$_T$m3+^{,Y}b3+ ^{n}anoparticles: the effect of the environment on light emissions. *J. Mater. Chem. C* **2015**, *3*, 3108−3113.
(24) Wang, F.; Banerjee, D.; Liu, Y.; Chen, X.; Liu, X. Upconversion nanoparticles in biological labeling, imaging, and therapy. *Analyst* **2010**, *135*, 1839−1854.
(25) Wang, G.; Peng, Q.; Li, Y. Lanthanide-doped nanocrystals: synthesis, optical-magnetic properties, and applications. *Acc. Chem. Res.* **2011**, *44*, 322−332.
(26) Deng, M.; Wang, L. Unexpected luminescence enhancement of upconverting nanocrystals by cation exchange with well retained small particle size. *Nano Res.* **2014**, *7*, 782.
(27) Carlos, L. D.; Sá Ferreira, R. A.; de Zea Bermudez, V.; Ribeiro, S. J. L. Lanthanide-containing light-emitting organic−inorganic hybrids: a bet on the future. *Adv. Mater.* **2009**, *21*, 509−534.
(28) Brites, C. D. S.; Lima, P. P.; Silva, N. J. O.; Millán, A.; Amaral, V. S.; Palacio, F.; Carlos, L. D. Lanthanide-based luminescent molecular thermometers. *New J. Chem.* **2011**, *35*, 1177−1183.
(29) Pedroni, M.; Piccinelli, F.; Passuello, T.; Giarola, M.; Mariotto, G.; Polizzi, S.; Bettinelli, M.; Speghini, A. Lanthanide doped upconverting colloidal CaF_2 nanoparticles prepared by a single-step hydrothermal method: toward efficient materials with near infrared-to-near infrared upconversion emission. *Nanoscale* **2011**, *3*, 1456−1460.
(30) Yu, M.; Li, F.; Chen, Z.; Hu, H.; Zhan, C.; Yang, H.; Huang, C. Laser scanning up-conversion luminescence microscopy for imaging cells labeled with rare-earth nanophosphors. *Anal. Chem.* **2009**, *81*, 930−935.
(31) Liu, Q.; Feng, W.; Yang, T.; Yi, T.; Li, F. Upconversion luminescence imaging of cells and small animals. *Nat. Protoc.* **2013**, *8*, 2033−2044.
(32) Dai, Y.; Xiao, H.; Liu, J.; Yuan, Q.; Ma, P. a.; Yang, D.; Li, C.; Cheng, Z.; Hou, Z.; Yang, P.; Lin, J. In vivo multimodality imaging and cancer therapy by near-infrared light-triggered trans-platinum pro-drug-conjugated upconverison nanoparticles. *J. Am. Chem. Soc.* **2013**, *135*, 18920−18929.
(33) Hou, Z.; Zhang, Y.; Deng, K.; Chen, Y.; Li, X.; Deng, X.; Cheng, Z.; Lian, H.; Li, C.; Lin, J. UV-emitting upconversion-based TiO_2 photosensitizing nanoplatform: near-infrared light mediated in vivo photodynamic therapy via mitochondria-involved apoptosis pathway. *ACS Nano* **2015**, *9*, 2584−2599.
(34) Zhang, P.; Steelant, W.; Kumar, M.; Scholfield, M. Versatile photosensitizers for photodynamic therapy at infrared excitation. *J. Am. Chem. Soc.* **2007**, *129*, 4526−4527.
(35) Chatterjee, D. K.; Yong, Z. Upconverting nanoparticles as nanotransducers for photodynamic therapy in cancer cells. *Nanomedicine* **2008**, *3*, 73−82.
(36) Qian, H. S.; Guo, H. C.; Ho, P. C.-L.; Mahendran, R.; Zhang, Y. Mesoporous-silica-coated up-conversion fluorescent nanoparticles for photodynamic therapy. *Small* **2009**, *5*, 2285−2290.
(37) Ungun, B.; Prud'homme, R. K.; Budijon, S. J.; Shan, J.; Lim, S. F.; Ju, Y.; Austin, R. Nanofabricated upconversion nanoparticles for photodynamic therapy. *Opt. Express* **2008**, *17*, 80−86.
(38) Guo, H.; Qian, H.; Idris, N. M.; Zhang, Y. Singlet oxygen-induced apoptosis of cancer cells using upconversion fluorescent nanoparticles as a carrier of photosensitizer. *Nanomed. Nanotechnol. Biol. Med.* **2010**, *6*, 486−495.
(39) Shan, J.; Budijono, S. J.; Hu, G.; Yao, N.; Kang, Y.; Ju, Y.; Prud'homme, R. K. Pegylated Composite Nanoparticles Containing Upconverting Phosphors and meso-Tetraphenyl porphine (TPP) for Photodynamic Therapy. *Adv. Funct. Mater.* **2011**, *21*, 2488−2495.
(40) Liu, J.; Bu, W.; Pan, L.; Shi, J. NIR-triggered anticancer drug delivery by upconverting nanoparticles with integrated azobenzene-modified mesoporous silica. *Angew. Chem., Int. Ed.* **2013**, *52*, 1−6.
(41) Idris, N. M.; Gnanasammandhan, M. K.; Zhang, J.; Ho, P. C.; Mahendran, R.; Zhang, Y. *In vivo* photodynamic therapy using upconversion nanoparticles as remote-controlled nanotransducers. *Nat. Med.* **2012**, *18*, 1580−1585.

DOI: 10.1021/acsomega.8b02416
ACS Omega 2019, 4, 3169−3177

(42) Zhao, Z.; Han, Y.; Lin, C.; Hu, D.; Wang, F.; Chen, X.; Chen, Z.; Zheng, N. Multifunctional Core-Shell Upconverting Nanoparticles for Imaging and Photodynamic Therapy of Liver Cancer Cells. *Chem.—Asian J.* **2012**, *7*, 830−837.
(43) Qiao, X.-F.; Zhou, J.-C.; Xiao, J.-W.; Wang, Y.-F.; Sun, L.-D.; Yan, C.-H. Triple-functional core-shell structured upconversion luminescent nanoparticles covalently grafted with photosensitizer for luminescent, magnetic resonance imaging and photodynamic therapy in vitro. *Nanoscale* **2012**, *4*, 4611−4623.
(44) Wang, C.; Cheng, L.; Liu, Y.; Wang, X.; Ma, X.; Deng, Z.; Li, Y.; Liu, Z. Imaging-guided pH-sensitive photodynamic therapy using charge reversible upconversion nanoparticles under near-infrared light. *Adv. Funct. Mater.* **2013**, *23*, 3077−3086.
(45) Xu, B.; Zhang, X.; Huang, W.; Yang, Y.; Ma, Y.; Gu, Z.; Zhai, T.; Zhao, Y. Nd^{3+} sensitized dumbbell-like upconversion nanoparticles for photodynamic therapy application. *J. Mater. Chem. B* **2016**, *4*, 2776−2784.
(46) Liu, X.; Que, I.; Kong, X.; Zhang, Y.; Tu, L.; Chang, Y.; Wang, T. T.; Chan, A.; Löwik, C. W. G. M.; Zhang, H. In vivo 808 nm image-guided photodynamic therapy based on an upconversion theranostic nanoplatform. *Nanoscale* **2015**, *7*, 14914−14923.
(47) Chen, F.; Zhang, S.; Bu, W.; Chen, Y.; Xiao, Q.; Liu, J.; Xing, H.; Zhou, L.; Peng, W.; Shi, J. A uniform sub-50 nm-sized magnetic/upconversion fluorescent bimodal imaging agent capable of generating singlet oxygen by using a 980 nm laser. *Chem.—Eur. J.* **2012**, *18*, 7082−7090.
(48) Huang, Y.; Skripka, A.; Labrador-Páez, L.; Sanz-Rodríguez, F.; Haro-González, P.; Jaque, D.; Rosei, F.; Vetrone, F. Upconverting nanocomposites with combined photothermal and photodynamic effects. *Nanoscale* **2018**, *10*, 791−799.
(49) Xing, R.; Liu, K.; Jiao, T.; Zhang, N.; Ma, K.; Zhang, R.; Zou, Q.; Ma, G.; Yan, X. An Injectable Self-Assembling Collagen-Gold Hybrid Hydrogel for Combinatorial Antitumor Photothermal/Photodynamic Therapy. *Adv. Mater.* **2016**, *28*, 3669−3676.
(50) Donnelly, R. F.; Cassidy, C. M.; Loughlin, R. G.; Brown, A.; Tunney, M. M.; Jenkins, M. G.; McCarron, P. A. Delivery of methylene blue and meso-tetra (N-methyl-4-pyridyl) porphine tetra tosylate from cross-linked poly(vinyl alcohol) hydrogels: a potential means of photodynamic therapy of infected wounds. *J. Photochem. Photobiol.* **2009**, *96*, 223−231.
(51) Hah, H. J.; Kim, G.; Lee, Y.-E. K.; Orringer, D. A.; Sagher, O.; Philbert, M. A.; Kopelman, R. Methylene blue-conjugated hydrogel nanoparticles and tumor-cell targeted photodynamic therapy. *Macromol. Biosci.* **2010**, *11*, 90−99.
(52) Meesaragandla, B.; Mahalingam, V. Synthesis of Upconverting Hydrogel Nanocomposites Using Thiol-Ene Click Chemistry: Template for the Formation of Dendrimer-Like Gold Nanoparticle Assemblies. *Chem.—Eur. J.* **2015**, *21*, 16811−16817.
(53) Krämer, K. W.; Biner, D.; Frei, G.; Güdel, H. U.; Hehlen, M. P.; Lüthi, S. R. Hexagonal sodium yttrium fluoride based green and blue emitting upconversion phosphors. *Chem. Mater.* **2004**, *16*, 1244−1251.
(54) Wang, F.; Liu, X. Recent advances in the chemistry of lanthanide-doped upconversion nanocrystals. *Chem. Soc. Rev.* **2009**, *38*, 976−989.
(55) Zhao, J.; Lu, Z.; Yin, Y.; McRae, C.; Piper, J. A.; Dawes, J. M.; Jin, D.; Goldys, E. M. Upconversion luminescence with tunable lifetime in $NaYF_4$:Yb,Er nanocrystals: role of nanocrystal size. *Nanoscale* **2013**, *5*, 944−952.
(56) Redmond, R. W.; Gamlin, J. N. A compilation of singlet oxygen yields from biologically relevant molecules. *Photochem. Photobiol.* **1999**, *70*, 391−475.

DOI: 10.1021/acsomega.8b02416
ACS Omega 2019, 4, 3169−3177